

## **General Disclaimer**

### **One or more of the Following Statements may affect this Document**

- This document has been reproduced from the best copy furnished by the organizational source. It is being released in the interest of making available as much information as possible.
- This document may contain data, which exceeds the sheet parameters. It was furnished in this condition by the organizational source and is the best copy available.
- This document may contain tone-on-tone or color graphs, charts and/or pictures, which have been reproduced in black and white.
- This document is paginated as submitted by the original source.
- Portions of this document are not fully legible due to the historical nature of some of the material. However, it is the best reproduction available from the original submission.

**NASA TECHNICAL  
MEMORANDUM**

NASA TM-73794

NASA TM-73794

(NASA-TM-73794) FORMATION OF Na<sub>2</sub>SO<sub>4</sub> AND  
K<sub>2</sub>SO<sub>4</sub> IN FLAMES DOPED WITH SULFUR AND ALKALI  
CHLORIDES AND CARBONATES (NASA) 19 p HC  
A02/MF A01 CSCL 21B

N78-13157

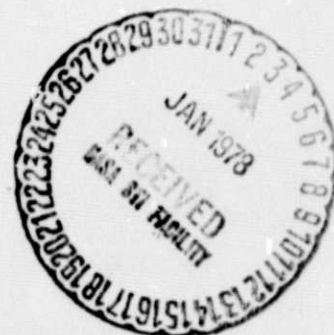
Unclas  
55202

G3/25

**FORMATION OF Na<sub>2</sub>SO<sub>4</sub> AND K<sub>2</sub>SO<sub>4</sub> IN FLAMES DOPED WITH  
SULFUR AND ALKALI CHLORIDES AND CARBONATES**

by George C. Fryburg, Robert A. Miller, Carl A. Stearns, and Fred J. Kohl  
Lewis Research Center  
Cleveland, Ohio 44135

TECHNICAL PAPER presented at the  
Symposium on High Temperature Metal Halide Chemistry  
sponsored by the Electrochemical Society  
Atlanta, Georgia, October 9-14, 1977



FORMATION OF Na<sub>2</sub>SO<sub>4</sub> AND K<sub>2</sub>SO<sub>4</sub> IN FLAMES DOPED WITH  
SULFUR AND ALKALI CHLORIDES AND CARBONATES

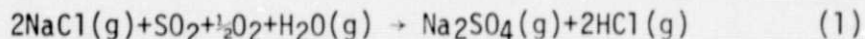
George C. Fryburg, Robert A. Miller,\* Carl A. Stearns,  
and Fred J. Kohl  
National Aeronautics and Space Administration  
Lewis Research Center  
Cleveland, Ohio 44135

ABSTRACT

High pressure, free-jet expansion, mass spectrometric sampling was used to identify directly and to measure reaction products formed in doped methane-oxygen flames. Flames were doped with SO<sub>2</sub> or CH<sub>3</sub>SH and sodium or potassium chlorides or carbonates. Gaseous Na<sub>2</sub>SO<sub>4</sub> or K<sub>2</sub>SO<sub>4</sub> molecules were formed in residence times on the order of 1 msec for each combination of dopants used. Composition profiles of combustion products were measured and compared with equilibrium thermodynamic calculations of product composition.

INTRODUCTION

The formation of alkali sulfates in combustion processes is of fundamental importance in understanding the high temperature corrosion that occurs in turbine engines, boilers, and magneto-hydrodynamic systems. It is well documented that sodium sulfate is one of the major reactants involved in the hot corrosion of turbine engine components (refs. 1-3). Generally, it has been assumed that sulfur impurities in the fuel and sodium chloride contained in the ingested air react during combustion to yield gaseous sodium sulfate (refs. 1 and 4):



The Na<sub>2</sub>SO<sub>4</sub>(g) has been postulated to condense on engine hot gas path parts under certain specific conditions (refs. 5 and 6).

Our high temperature Knudsen cell, mass spectrographic investigation of the vaporization of sodium sulfate (ref. 6) has lent credence to reaction (1) by establishing the existence of the Na<sub>2</sub>SO<sub>4</sub>(g) molecule and by providing values for its thermodynamic properties.

---

\* NRC Resident Research Associate.

Using the data for  $\text{Na}_2\text{SO}_4(\text{g})$  and for other pertinent molecular species ( $\text{NaCl}(\text{g})$ ,  $\text{NaOH}(\text{g})$ ,  $\text{SO}_2(\text{g})$ ,  $\text{SO}_3(\text{g})$ ,  $\text{HCl}(\text{g})$ , etc.) we were able to obtain thermodynamic descriptions of the equilibria possible in various combustion systems of practical interest (ref. 6). The results of such calculations predict that under equilibrium conditions, gaseous sodium sulfate should be formed in suitably doped burner rigs and in turbine engines operating under their usual environmental conditions.

To validate these thermochemical predictions, we have been investigating the formation of sodium sulfate in Mach 0.3 atmospheric pressure, burner rigs and in laboratory type, flat-flame burners. Recently, we reported our burner rig results (ref. 7) for Jet A fuel doped with 8 ppm NaCl. Deposits were collected on cylindrical platinum targets placed in the combustion products, and the deposition was studied as a function of collector temperature. Experimental deposition onset temperatures checked, within experimental error, with predicted temperatures calculated from thermochemical data. In addition, it was shown that the deposits were crystalline  $\text{Na}_2\text{SO}_4$  with no chloride detectible above background levels. The residence time in the burner rig was 2.2 msec, indicating that conversion of NaCl to  $\text{Na}_2\text{SO}_4$  could occur in the time frame encountered in modern day jet aircraft turbine engines, which is in the range 5 to 10 msec.

In our flat-flame burner studies, we have employed fuel-lean  $\text{CH}_4\text{-O}_2$  flames doped with sulfur and alkali metal salts. Identification of products is effected by high pressure, free-jet expansion, modulated molecular beam mass spectrometric sampling (ref. 8). Recently, we reported results (ref. 9) for a flame doped with  $\text{SO}_2$  and NaCl. We were able to identify  $\text{Na}_2\text{SO}_4(\text{g})$  molecules in the flame.

This paper describes additional studies investigating the kinetics of formation of  $\text{Na}_2\text{SO}_4$ , and also of  $\text{K}_2\text{SO}_4$ , in  $\text{CH}_4\text{-O}_2$  flames doped with  $\text{SO}_2$  or  $\text{CH}_3\text{SH}$ , and with NaCl,  $\text{Na}_2\text{CO}_3$ , KCl, or  $\text{K}_2\text{CO}_3$ . Experimental results are compared with calculated thermochemical predictions.

## EXPERIMENTAL

The experimental system used to study the formation of gaseous alkali metal sulfates consisted of a premixed, laminar flow flat-flame that could be sampled by a high pressure, modulated molecular beam, mass spectrometric sampler. A schematic of the experimental arrangement is given in figure 1.

The flat flame burner, shown in more detail in figure 2, was operated at atmospheric pressure. Fuel-lean  $\text{CH}_4\text{-O}_2$  flames were employed. The fuel could be doped either with  $\text{CH}_3\text{SH}$  or  $\text{SO}_2$ , and the oxygen could be doped with alkali salts by aspiration of water solutions. Gas flow rates were regulated with needle valves and measured with calibrated rotometers. Nebulization rates were determined by

measuring the rate of solution aspiration and the rate of return of liquid recovered from the mixing chamber. Total gas flow through the burner was on the order of  $111 \text{ min}^{-1}$  (STP). Reactant gases were mixed in the mixing chamber and the resulting mixture passed through a series pair of flow straighteners 2.5 cm in diameter and 1.25 cm long. The flow straighteners were honeycombs fabricated from Hastelloy-X with openings 0.08 cm on a side which resulted in 135 openings per square centimeter. Upon ignition, the combustible mixture burned in a plane slightly above the top flow straightener. The flame was screened from the ambient atmosphere by a  $31 \text{ min}^{-1}$  circumferential laminar flow of nitrogen emanating from a flow straightener situated around the water-cooled combustible mixture flow pipe. The screen-gas flow straightener was 1.25 cm long with inside and outside diameters of 2.5 and 5 cm, respectively.

A typical flame is shown in figure 3. The flame had a luminous zone thickness of about one millimeter and was located somewhat less than one millimeter above the top surface of the burner. The burner was supported by mechanical devices that facilitated micrometer movement in three mutually perpendicular directions. The vertical distance, perpendicular to the flame front, between the surface of the burner and the inlet orifice of the mass spectrometric sampler, was denoted Z. The distance Z could be varied in the range 0.3 to 25 mm and measured with a precision of 0.025 mm.

Direct mass spectrometric analysis of the species in the atmospheric pressure flames was accomplished with a high pressure, free-jet expansion, modulated molecular beam mass spectrometric sampler. The technique is used to sample directly the species while preserving their dynamic and chemical integrity (ref. 8). Our sampler, described in more detail in reference 8, is shown schematically in figure 4. Atmospheric pressure sampling was accomplished by free-jet expansion through a 0.22 mm diameter orifice in the apex of a 0.3 cm high sampling cone. The conductance of the orifice was around  $200 \text{ cc min}^{-1}$  (STP) at the flame temperatures employed in this study. The cone was fabricated from 0.25 mm thick Pt 10%Rh and had an included angle of  $106^\circ$ . The sampling cone was welded to a 2 cm diameter by 1.5 cm long stainless steel tube.

The center portion of the expanded beam from the sampling orifice was skimmed by a skimmer cone with an orifice diameter of 0.81 mm and an included angle of  $60^\circ$ . The distance between the sampling orifice and skimmer orifice was 3.17 cm. For this physical configuration, with the nominal pumping speeds indicated in figure 4, first and second stage pressures were approximately  $1.5 \times 10^{-3}$  torr and  $8 \times 10^{-6}$  torr, respectively, when sampling room temperature, atmospheric pressure gas. When the gas temperature was increased to  $1000^\circ\text{C}$ , these pressures were  $7 \times 10^{-4}$  torr and  $1 \times 10^{-6}$  torr, respectively. Third and fourth stage pressures were always less than  $10^{-7}$  and  $10^{-8}$  torr, respectively, for all sampling conditions. Stage 1 pressures were read

with a capacitance manometer, and the pressures in the other three stages were read with ion gauges.

The molecular beam from the skimmer was chopped by a motor driven two-toothed chopper wheel located in Stage II. A chopping frequency of 150 hertz was used and a reference signal at this frequency was derived from a light bulb and photodiode coupled to the chopper wheel. The chopped molecular beam then passed to the electron bombardment ion source of a quadrupole mass spectrometer (Extranuclear Laboratories). The high efficiency ion source was operated with a current of approximately 3 mA of 30 eV electrons. The quadrupole filter with 1.6 cm diameter poles had a mass range extending to over 600 AMU. A Channeltron electron multiplier was employed to multiply the ion current output of the ion source-quadrupole filter. Two channels of output current were measured as a function of quadrupole filter tuning. One channel measured the total chopped ion current, and the other channel measured only the component of the ion current signal in phase with the chopper. The second channel was driven by a lock-in amplifier, phase sensitive detector system tuned to the chopper frequency reference signal.

The gaseous species in various flame systems were measured by recording the in-phase component of the ion current for respective values of mass-to-charge ratio,  $m/e$ . The experimental results presented here are considered to be qualitatively correct but quantitative aspects are considered to be preliminary. The measured ion intensities have not been adjusted to account for mass discrimination resulting from Mach-number focusing (refs. 10, 11, and 12), quadrupole mass filter transmission (ref. 13), or multiplier gain variations as a function of  $m/e$ . Factors such as these are best accounted for by performing *in situ* calibrations (e.g., see ref. 14); such calibrations have not yet been performed for our experiments. Ion intensities reported here have, however, been corrected for relative ionization cross sections. Cross sections for atoms were taken from Mann (ref. 15) and estimated for molecules as 0.75 times the sum of the atomic values. During operation of the complex flat flame burner-mass spectrometric system, problems of clogging of the sampler inlet orifice and of the aspirator-nebulizer were encountered frequently. These problems limited the duration of each flame experiment and thus the amount of data that could be obtained.

## RESULTS AND DISCUSSION

Mass Spectrometric Sampler Experiments. - Five separately doped  $\text{CH}_4\text{-O}_2$  flame systems were investigated. The reactant gas compositions are given in Table I along with the calculated adiabatic flame temperatures and the flame speeds. We were able to identify the appropriate gaseous alkali sulfate molecule in each flame system. In addition, composition profiles for various gaseous species as a function of  $Z$

were obtained for the NaCl-SO<sub>2</sub> and the K<sub>2</sub>CO<sub>3</sub>-SO<sub>2</sub>-doped flames. These results are given in figures 5 and 6. The results for the NaCl-SO<sub>2</sub>-doped flame have been described in a recent communication (ref. 9) but are presented here for ease of comparison.

The molecules shown in figures 5 and 6 were monitored by measuring the ion intensities of the respective molecular ions. The composition profiles obtained for the major species O<sub>2</sub>, H<sub>2</sub>O, and CO<sub>2</sub> are generally similar to those reported for CH<sub>4</sub>-O<sub>2</sub> flames (ref. 16). For the alkali metal- and sulfur-containing species, the observed profile shapes seem reasonable. However, Na<sub>2</sub>SO<sub>4</sub>(g) and K<sub>2</sub>SO<sub>4</sub>(g) exhibited a drop in intensity from the peak as Z increased, and a subsequent rise with further increase in Z. This behavior may have resulted from the fact that the stability of the gaseous alkali sulfates is a very sensitive function of temperature, increasing with decreasing temperature. Thus, several factors may have pronounced effects on the intensity of the gaseous sulfates: (1) cooling of the flame by the sampling cone, for small Z values; (2) variation of flame temperature as a function of Z; and (3) existence of regions of super saturation for these species.

For the NaCl-SO<sub>2</sub>-doped flame (fig. 5) two stable intermediate molecules were detected; i.e., NaSO<sub>2</sub> and NaSO<sub>3</sub>. These species are considered to be reaction intermediates because their respective ions were not observed as fragments in our Knudsen cell vaporization of Na<sub>2</sub>SO<sub>4</sub> (ref. 6). The composition profiles of these intermediates displayed peaks similar to the Na<sub>2</sub>SO<sub>4</sub>(g) at small Z values, and may have resulted from the same factors that account for the Na<sub>2</sub>SO<sub>4</sub>(g) profile.

For the K<sub>2</sub>CO<sub>3</sub>-SO<sub>2</sub>-doped flame (fig. 6) no reaction intermediates could be observed. Experimental problems associated with "metastable noise" (ref. 17) in the mass spectrometer prevented identification of these intermediates.

No attempt was made to make intensity measurements at values of Z less than 0.3 mm because it was observed that at very small values of Z there was a decrease in total ion intensity. This is probably due to probe interactions. The ramifications of various flame-sampling probe interactions have been considered in detail by Biordi et al. (refs. 14 and 18) and Hayhurst et al. (refs. 19 and 20). The composition profiles shown in figure 5 and 6 indicate that Na<sub>2</sub>SO<sub>4</sub>(g), K<sub>2</sub>SO<sub>4</sub>(g), NaSO<sub>2</sub>(g), and NaSO<sub>3</sub>(g) are formed very early in the flame. Residence times were calculated on the basis of flow velocities determined for the total flow of unreacted cold gas. On this basis we estimate that the species Na<sub>2</sub>SO<sub>4</sub>(g), K<sub>2</sub>SO<sub>4</sub>(g), NaSO<sub>2</sub>(g), and NaSO<sub>3</sub>(g) are formed in residence times of less than one millisecond.

The residence time for the formation of Na<sub>2</sub>SO<sub>4</sub>(g) in the NaCl-SO<sub>2</sub>-doped flames is quite short. However, sulfur impurities in fuels generally occur as sulfide sulfur. Evidence indicates that the

oxidation of sulfide sulfur to  $\text{SO}_2$  is very rapid in flames (ref. 21). Nevertheless, because of the small time frame involved, we investigated a  $\text{NaCl-CH}_3\text{SH}$ -doped flame. The  $\text{Na}_2\text{SO}_4(\text{g})$  was readily observed at a value of  $Z$  that corresponded to a gas transit time from the top of the burner to the point of sampling of 1.1 msec. Clogging of the sampling orifice was a severe problem with this flame. As a result, only short times were available for measuring ion intensities, and no positive identifications could be made of  $\text{NaSO}_2^+$  or  $\text{NaSO}_3^+$ -ions which would have required large time constants and long scan times for their measurement. The point to be emphasized is that  $\text{Na}_2\text{SO}_4(\text{g})$  was formed from the sulfide sulfur in the  $\text{CH}_3\text{SH-NaCl}$  system in about the same time frame as in the  $\text{SO}_2\text{-NaCl}$  system.

Calculation of Flame Compositions. - To facilitate a comparison of experimental observations with equilibrium thermodynamic predictions, we calculated the mole fractions of flame reaction products. The calculations were performed with the NASA complex chemical equilibrium computer program (ref. 22) which has been described in detail previously. This program is based on the minimization of free energy approach to chemical equilibrium calculations subject to the constraint of maintaining a proper mass balance between reactants and products. The program permits the calculation of chemical equilibrium composition for homogeneous or heterogeneous systems for assigned thermodynamic states such as temperature-pressure (T,P) and enthalpy-pressure (H,P). For the present work, the role of  $\text{Na}_2\text{SO}_4$  (c or g) or  $\text{K}_2\text{SO}_4$  (c or g) in typical doped methane-oxygen flames was examined by obtaining results describing flame temperatures and compositions as a function of fuel-to-oxidant mass ratio. For the calculations, the convention used was that  $\text{CH}_4$  and  $\text{SO}_2$  or  $\text{CH}_3\text{SH}$  were labeled fuel and  $\text{O}_2$ ,  $\text{H}_2\text{O}$ , and the alkali metal salt were labeled oxidant. Calculations were made for each of the flame systems listed in Table I. The equilibrium compositions of the reacted flame gases and the adiabatic flame temperatures are presented in figure 7(a) for the major products and in figure 7(b) for the sodium-containing species for the  $\text{NaCl-SO}_2$ -doped flame. Figures 8 to 11 show the results for the alkali metal-containing species for the remainder of the flame systems listed in Table I. The major products for all of these flames are almost identical to those for the  $\text{NaCl-SO}_2$  system and are not repeated. To arrive at the distributions of molecular species depicted in these figures, the program considered simultaneously over 70 gaseous and condensed species made up of C-H-O-S-M-Cl combinations, where M = Na or K. The thermodynamic data for most of these species was obtained from the JANAF tables (ref. 23). The data for  $\text{Na}_2\text{SO}_4(\text{g})$  were taken from reference 6 and the data for  $\text{K}_2\text{SO}_4(\text{g})$  were calculated on the basis of estimated molecular parameters and the heat of formation of  $\text{K}_2\text{SO}_4(\text{g})$  from the work of Halstead (ref. 24). It must be pointed out that only those molecular species for which the program was given thermodynamic data were considered in the calculations; no data for species such as

NaSO<sub>2</sub> or NaSO<sub>3</sub> were included.

The results of the calculations show that sodium or potassium are distributed in complex patterns between M<sub>2</sub>SO<sub>4</sub>(c), MCl(g), MOH(g), M<sub>2</sub>SO<sub>4</sub>(g) and M(g). At low values of the fuel/oxidant ratios (corresponding to low flame temperatures) and up to sharp cut-off points, the alkali metals are tied up almost exclusively as M<sub>2</sub>SO<sub>4</sub>(c). Gaseous M<sub>2</sub>SO<sub>4</sub> is present in significant amounts over a relatively narrow range of fuel/oxidant ratios and always at molar concentrations of less than 10% of MCl(g) for Cl-containing systems. At high fuel/oxidant ratios, MOH(g), M(g), and MCl(g) account for most of the alkali metal.

Experimental results for the NaCl-SO<sub>2</sub> and K<sub>2</sub>CO<sub>3</sub>-SO<sub>2</sub> flames are compared with the calculations by plotting the calculated mole fraction of products on the right-hand sides of figures 5 and 6. At the outset one must recognize that two factors prevail: (1) as noted earlier, the experimental results were not "calibrated," and (2) the calculations are for equilibrium conditions. With these factors in mind, the agreement between experiment and calculation is considered to be good for the species O<sub>2</sub>, H<sub>2</sub>O, CO<sub>2</sub>, SO<sub>2</sub>, and SO<sub>3</sub>, all of which are only slowly varying functions of the fuel/oxidant ratio. For the remaining experimentally measured species other factors must be considered. These factors include: (1) the fuel/oxidant ratio given for the experimental flame has uncertainty associated with it due mainly to the method used to introduce the alkali containing salt, (2) most of the alkali metal and sulfur-containing species are critically dependent on the fuel/oxidant ratio, (3) the stability both of Na<sub>2</sub>SO<sub>4</sub>(g) and K<sub>2</sub>SO<sub>4</sub>(g) are rapidly varying functions of temperature, and (4) the experimental flame temperatures are expected to be significantly below the calculated adiabatic flame temperature of 2032 K and 2101 K. We calculate that if the NaCl-SO<sub>2</sub> flame were 200° cooler, the predicted level of Na<sub>2</sub>SO<sub>4</sub>(g) would equal the experimental level. In the next section, temperature profiles are described giving insight to this problem. By reflecting on all the factors to be considered, we conclude that the agreement between experiment and calculation is reasonable and that the calculations are useful in predicting at least qualitatively what is to be expected in experimental flame systems.

Temperature Measurements. - The flames used in this investigation have been further characterized by temperature measurements in a salt- and sulfur-free, methane-oxygen flame. Thermocouples (Pt-Pt 13%Rh) were used to profile temperature as a function of vertical distance above the burner and other temperature measurements were made to assess the extent of cooling by the sampler. The measurements reported in this paper were made with a stirrup-shaped thermocouple [patterned after the design of Biordi et al. (ref. 18)] formed from 5 mil wire with a 10 mil diameter junction. Some attempts were made to use one-mil butt-welded thermocouples, but these proved to be too fragile to use continuously for our flame temperature and velocity. The temperatures

that were measured by the one mil thermocouples were over  $100^{\circ}\text{C}$  higher than those measured by the larger diameter thermocouples. This temperature was higher because less heat is lost by radiation from the smaller diameter wire. Several expressions have been suggested for correcting for radiative heat loss, but all of these give somewhat different results, as will be discussed later. The temperatures that are to be reported here have not been corrected. Attempts have been made to prevent heating of the thermocouples by catalytic recombination of atoms on their surfaces. To do this, a layer of silica was deposited on the wires by dipping them in silicone oil (DC703), and then burning in a Bunsen burner flame. This coating appeared to lower the measured temperature by about  $10^{\circ}\text{C}$ .

Plots of the uncorrected temperature data are given in figure 12(a) and (b). In figure 12(a), the thermocouple temperature is plotted as a function of its distance above the burner surface, and it is seen that in the regions investigated the temperature dropped continuously as distance increased. The large drop at 29.5 mm appears to be due to invasion of the flame by the ambient atmosphere. In figure 12(b), the distance from the thermocouple to the burner is fixed and the temperature is recorded as a function of the distance,  $Z$ , from the burner surface to the sampling orifice. The distance at which the thermocouple would touch the orifice is denoted by the vertical line at distance  $D$ . In this plot, as  $Z$  decreases the temperature is seen to drop because of heat lost to the sampling probe and its flange. At distances very close to the orifice some of the temperature drop is associated with the initial stages of the supersonic expansion. In a previous paper (ref. 8) we showed that the supersonic expansion can be expected to begin upstream from the orifice at an approximate distance of one orifice diameter. Gases within this distance will be rapidly sampled, and therefore one can assume that the molecules entering the sampler are characteristic of the flame at that point. In figure 12(b), the difference between the temperature at one orifice diameter from the probe and the highest temperature measured is  $16^{\circ}\text{C}$ . This value is about an order of magnitude less than the temperature drop reported for a low pressure flame (ref. 18). Thus, because of the relatively large volume flow rate characteristic of our flame, the cooling by the sampler does not appear to be a serious difficulty.

The adiabatic temperature of this flame is calculated to be 2271k. Actual flame temperatures are somewhat lower than the calculated value because of heat losses to the surroundings, but they are higher than the temperatures measured by thermocouples because of radiation losses from the hot wire. Several expressions are available for correcting for radiation losses. One such expression has been derived by Kashkan (ref. 25) and its use has been recommended by Fristrom and Westenburg (ref. 26) and by Biordi et al. (ref. 14). This expression considers convective heat transfer to the wire and radiative heat loss from the wire. Accordingly, it contains terms for the emissivity and

diameter of the wire (assumed to be cylindrical), and the viscosity, density, and velocity of the flame gases, most of these quantities must be estimated; in addition, our wire was not cylindrical because the junction was formed into a bead. However, the magnitude of the correction is such that the highest temperature recorded in figure 12 could be adjusted to about 2100K. Thus it appears that the flame temperature at the point of sampling could be about 200° lower than the adiabatic temperature, as discussed in the previous section.

#### CONCLUDING REMARKS

In summary, we have observed the formation of gaseous  $\text{Na}_2\text{SO}_4$  and  $\text{K}_2\text{SO}_4$  in methane-oxygen flames doped with sulfur-containing compounds ( $\text{SO}_2$  or  $\text{CH}_3\text{SH}$ ) and alkali metal salts ( $\text{NaCl}$ ,  $\text{Na}_2\text{CO}_3$ ,  $\text{KCl}$ , or  $\text{K}_2\text{CO}_3$ ). The  $\text{M}_2\text{SO}_4(\text{g})$  molecules were formed from either  $\text{SO}_2$  or  $\text{CH}_3\text{SH}$  in residence times on the order of 1 msec. Equilibrium thermodynamic calculations of flame reaction products showed that the alkali metal is distributed in a complex way as a function of fuel-to-oxidant ratio between sulfate, chloride, hydroxide, and gaseous metal species. The experimentally determined product mole fractions are in reasonable agreement with the calculated values.

That the  $\text{M}_2\text{SO}_4(\text{g})$  species, predicted by the equilibrium thermodynamic calculations, was observed experimentally in short residence times is of fundamental significance to the hot corrosion problem. The result corroborates our burner-rig results in which we observed deposition of  $\text{Na}_2\text{SO}_4(\text{c})$  from combustion gases in a  $\text{NaCl}$ -doped Jet A-air flame (ref. 7) in residence times of 2.2 msec.

These observations are different from Hanby's (ref. 27) finding that residence times of greater than 8 msec were required for formation of  $\text{Na}_2\text{SO}_4$  in combustion gases. Critical analysis of Hanby's results is complicated by the difficulty of determining the fuel/air ratio in different sections of the combustor. Apparently,  $\text{Na}_2\text{SO}_4$  was detected only after the fuel/air ratio of the combustion products was changed by addition of dilution cooling air. This situation makes definition of the residence time uncertain.

Our findings, obtained in widely differing experimental set-ups with well-defined conditions, verify that gaseous  $\text{Na}_2\text{SO}_4$  can be formed in turbine engines by reaction of ingested  $\text{NaCl}$  with sulfur impurities in fuels.

#### REFERENCES

1. J. Stringer, MCIC 72-08, Metals and Ceramics Information Center, Columbus, OH (1972).

2. N. S. Bornstein, M. A. DeCrescente, and H. A. Roth, in "Proceedings of the 1972 Tri-Service Conference on Corrosion," MCIC 73-19, M. M. Jacobson and A. Gallaccio, Editors, p. 15, Metals and Ceramics Information Center, Columbus, OH (1973).
3. J. A. Goebel and F. S. Pettit, in "Metal-Slag-Gas Reactions and Processes," Z. A. Foroulis and W. W. Smeltzer, Editors, p. 693, The Electrochemical Society Softbound Symposium Series, Princeton, NJ (1975).
4. J. F. G. Condé, in "High Temperature Corrosion of Aerospace Alloys," AGARD-CP-120, J. Stringer, R. I. Jaffee, and T. F. Kearns, Editors, p. 204, Advisory Group for Aerospace Research and Development, France (1972).
5. N. S. Bornstein and M. A. DeCrescente, *Corrosion* 24, 127 (1968).
6. F. J. Kohl, C. A. Stearns, and G. C. Fryburg, in "Metal-Slag-Gas Reactions and Processes," Z. A. Foroulis and W. W. Smeltzer, Editors, p. 649, The Electrochemical Society Softbound Symposium Series, Princeton, NJ (1975); also NASA TM X-71641 (1975).
7. F. J. Kohl, G. J. Santoro, C. A. Stearns, G. C. Fryburg, and D. E. Rosner, NASA TM X-73683 (1977).
8. C. A. Stearns, F. J. Kohl, G. C. Fryburg, and R. A. Miller, NASA TM 73720 (1977).
9. C. A. Stearns, R. A. Miller, F. J. Kohl, and G. C. Fryburg, *J. Electrochem. Soc.* 124, 1145 (1977); also NASA TM X-73600 (1977).
10. J. B. Anderson, in "Molecular Beams and Low Density Gas Dynamics," P. P. Wegener, Editor, p. 1, Marcel-Dekker, Inc. NY (1974).
11. T. A. Milne, J. Brewer, and F. T. Greene, in "Proceedings of the First Meeting of the Interagency Chemical Rocket Propulsion Group, Working Group in Thermochemistry," Vol. 1, CPIA-44, p. 123, Chemical Propulsion Information Agency, Silver Springs, MD (1964).
12. P. K. Sharma, E. L. Kriuth, and W. S. Young, *J. Chem. Phys.* 64, 4345 (1976).
13. T. C. Ehlert, *J. Phys.*, Section E: *Sci. Inst.* 3, 237 (1970).
14. J. C. Biordi, C. P. Lazzara, J. F. Papp, Bureau of Mines, Pittsburgh, PA, BM-RI-7723 (1973).
15. J. B. Mann, in "Recent Developments in Mass Spectrometry," K. Ogata and T. Hayakawa, Editors, p. 814, Univ. Press, Baltimore, MD (1970).

16. J. Peeters and G. Mahnen, in "Fourteenth International Symposium on Combustion," p. 133, The Combust. Inst., Pittsburgh, PA (1973).
17. T. A. Milne and J. E. Beachey, Third Quarterly Progress Report, Oct. 1-Dec. 31, 1976, ERDA Contract No. E(49-18)-2288, Midwest Research Inst. Rept. No. FE-2288-12 (1977).
18. J. C. Biordi, C. P. Lazzara, and J. F. Papp, Combustion and Flame 23, 73 (1974).
19. A. N. Hayhurst, D. B. Kittleson, and N. R. Telford, Combustion and Flame 28, 123 (1977).
20. A. N. Hayhurst and D. B. Kittleson, Combustion and Flame 28, 137 (1977).
21. A. Levy, E. L. Merryman, and W. T. Reid, Environmental Science and Technology 4, 653 (1970).
22. S. Gordon and B. J. McBride, NASA SP-273 (1971).
23. JANAF Thermochemical Tables, Dow Chemical Co., Midland, MI.
24. W. D. Halstead, Trans. Faraday Soc. 66, 1 (1970).
25. W. E. Kaskan, "Sixth International Symposium on Combustion," p. 134, Reinhold Publishing Corp., NY (1957).
26. R. M. Fristrom and A. A. Westenberg, "Flame Structure," p. 424, McGraw-Hill, NY (1965).
27. V. I. Hanby, J. Eng. Power 96, 129 (1974).

TABLE I  
 ALKALI METAL- AND SULFUR-CONTAINING COMPOUND  
 ADDITIONS TO METHANE-OXYGEN FLAMES

Flame System	Reactant Gas Composition (mole %)		Fuel/Oxidant Mass Ratio	Calculated Adiabatic Flame Temperature (K)	Flame* Speed (cm sec <sup>-1</sup> )
	Fuel	Oxidant			
NaCl-SO <sub>2</sub>	8.9 CH <sub>4</sub>	84.1 O <sub>2</sub>	0.072	2032	45
	0.92 SO <sub>2</sub>	5.9 H <sub>2</sub> O 0.18 NaCl			
NaCl-CH <sub>3</sub> SH	5.3 CH <sub>4</sub>	87.3 O <sub>2</sub>	0.046	1678	43
	1.0 CH <sub>3</sub> SH	6.2 H <sub>2</sub> O 0.19 NaCl			
Na <sub>2</sub> CO <sub>3</sub> -SO <sub>2</sub>	9.3 CH <sub>4</sub>	83.6 O <sub>2</sub>	0.077	2097	44
	1.0 SO <sub>2</sub>	6.0 H <sub>2</sub> O 0.051 Na <sub>2</sub> CO <sub>3</sub>			
KCl-SO <sub>2</sub>	9.3 CH <sub>4</sub>	83.5 O <sub>2</sub>	0.076	2088	44
	1.0 SO <sub>2</sub>	6.0 H <sub>2</sub> O 0.19 KCl			
K <sub>2</sub> CO <sub>3</sub> -SO <sub>2</sub>	9.3 CH <sub>4</sub>	83.8 O <sub>2</sub>	0.075	2101	45
	0.92 SO <sub>2</sub>	5.9 H <sub>2</sub> O 0.025 K <sub>2</sub> CO <sub>3</sub>			

\* The flame speed,  $V_0$  in cm sec<sup>-1</sup>, was calculated on the basis of the NTP flow velocity of the reactant gases.

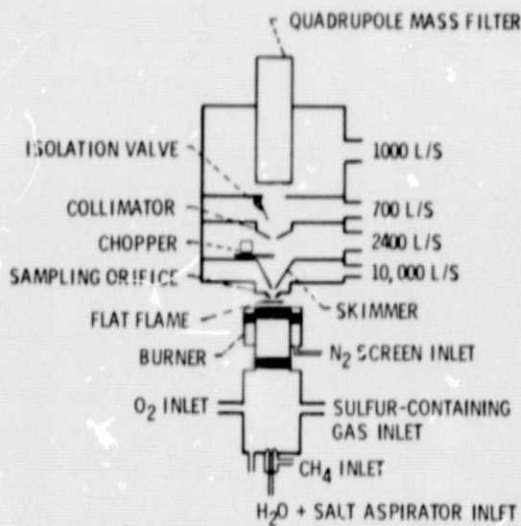


Figure 1. - Schematic of high pressure mass spectrometric flame sampling apparatus.

E-9362

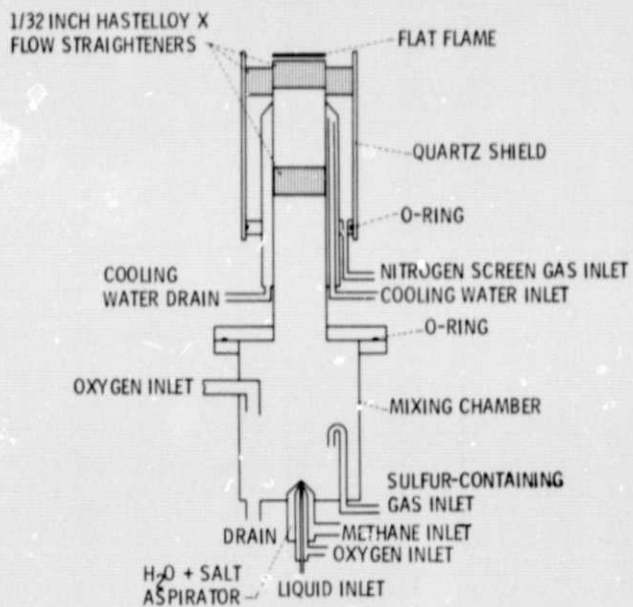
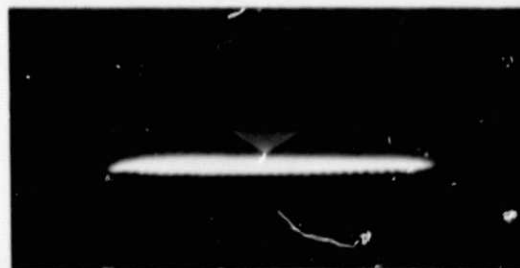
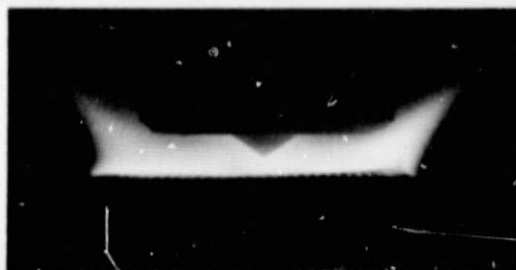


Figure 2. - Schematic of flat flame burner.



(a) WITHOUT NaCl



(b) WITH NaCl

Figure 3. - Photographs of flat flame.

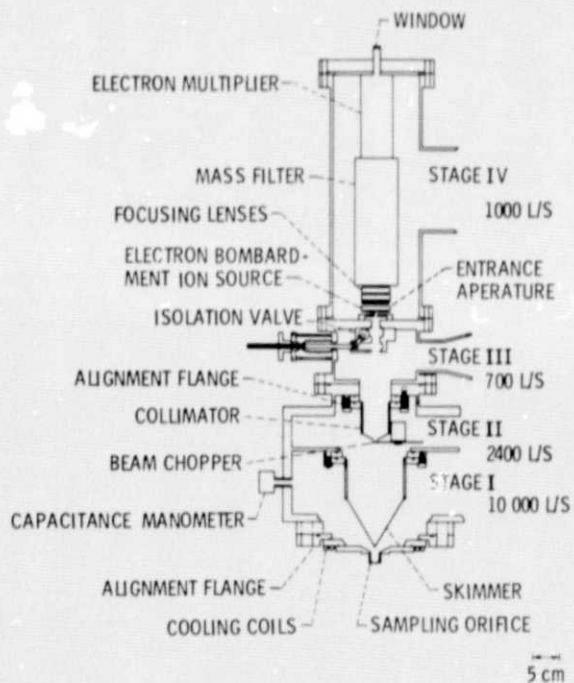


Figure 4. - Schematic cross section of high pressure mass spectrometric sampler.

ORIGINAL PAGE IS  
OF POOR QUALITY

ORIGINAL PAGE IS  
OF POOR QUALITY

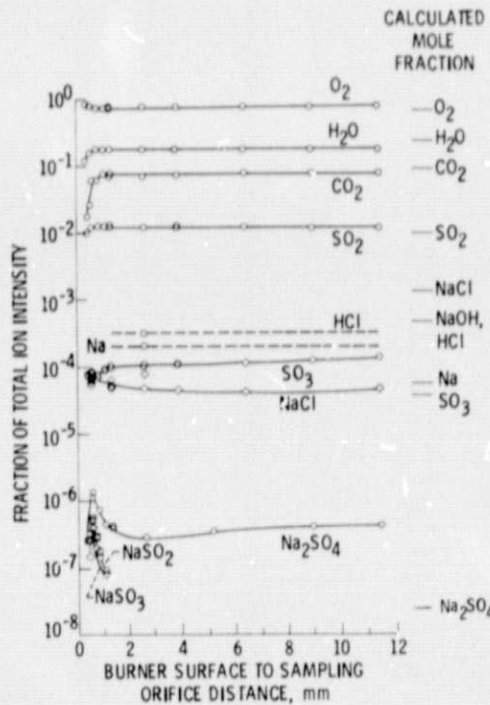


Figure 5. - Composition profiles for  $\text{CH}_4\text{-O}_2\text{-H}_2\text{O-NaCl-SO}_2$  flame. Reactants (mole %): 8.9  $\text{CH}_4$ , 84.1  $\text{O}_2$ , 5.9  $\text{H}_2\text{O}$ , 0.18  $\text{NaCl}$ , and 0.92  $\text{SO}_2$ . Calculated mole fractions refer to the adiabatic flame temperature.

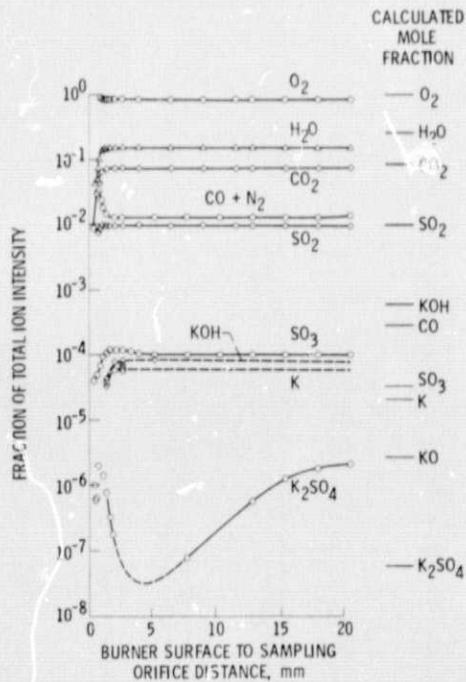


Figure 6. - Composition profiles for  $\text{CH}_4\text{-O}_2\text{-H}_2\text{O-K}_2\text{CO}_3\text{-SO}_2$  flame. Reactants (mole %): 9.3  $\text{CH}_4$ , 83.8  $\text{O}_2$ , 5.9  $\text{H}_2\text{O}$ , 0.025  $\text{K}_2\text{CO}_3$ , and 0.92  $\text{SO}_2$ . Calculated mole fractions refer to the adiabatic flame temperature.

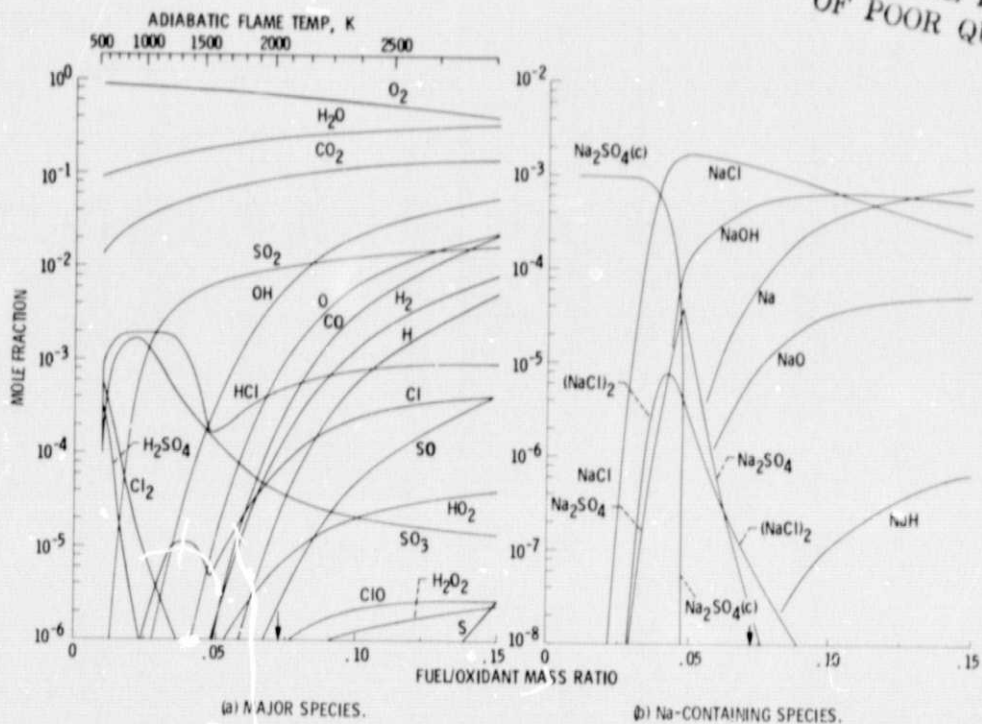


Figure 7. - Equilibrium chemical composition for NaCl- $SO_2$ -doped  $CH_4-O_2$  flame. Arrows indicate fuel/oxidant mass ratio of flame used.

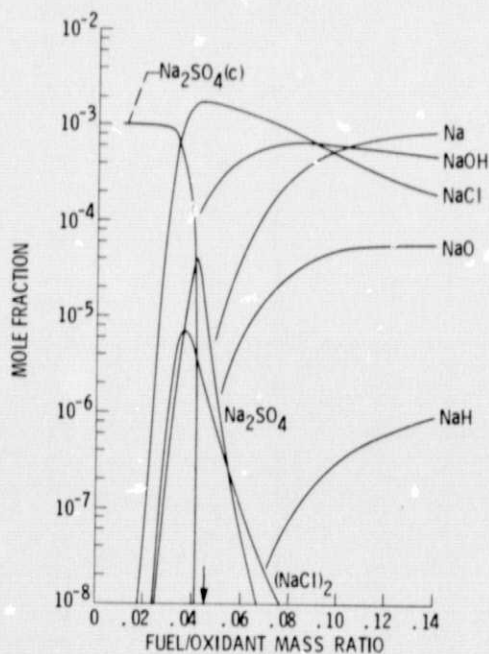


Figure 8. - Equilibrium chemical composition for NaCl- $CH_3SH$ -doped  $CH_4-O_2$  flame; sodium-containing species. Arrow indicates fuel/oxidant mass ratio of flame used.

ORIGINAL PAGE IS  
OF POOR QUALITY

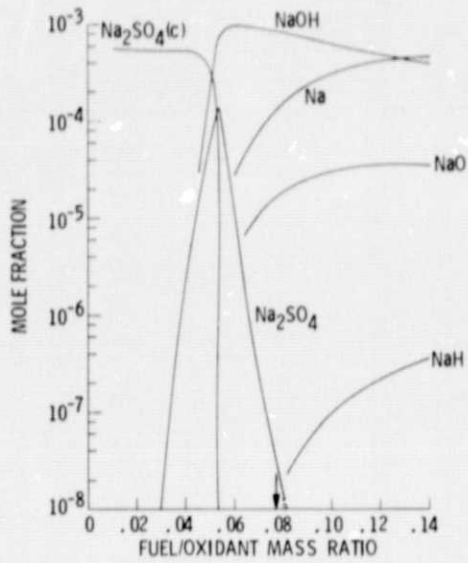


Figure 9. - Equilibrium chemical composition for  $\text{Na}_2\text{CO}_3\text{-SO}_2$ -doped  $\text{CH}_4\text{-O}_2$  flame; sodium-containing species. Arrow indicates fuel/oxidant mass ratio of flame used.

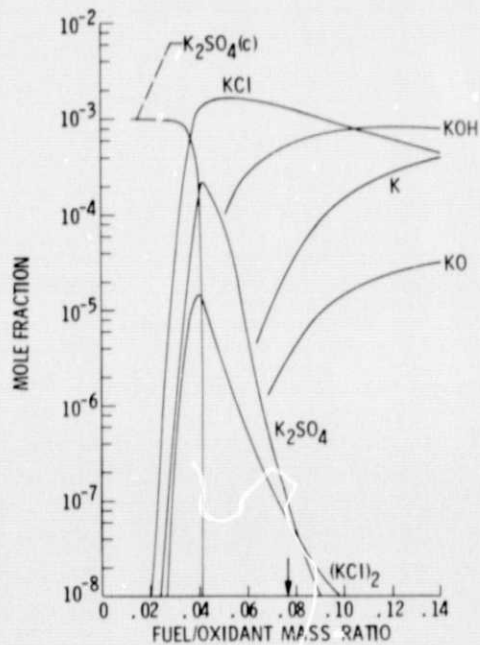


Figure 10. - Equilibrium chemical composition for  $\text{KCl-SO}_2$ -doped  $\text{CH}_4\text{-O}_2$  flame; potassium-containing species. Arrow indicates fuel/oxidant mass ratio of flame used.

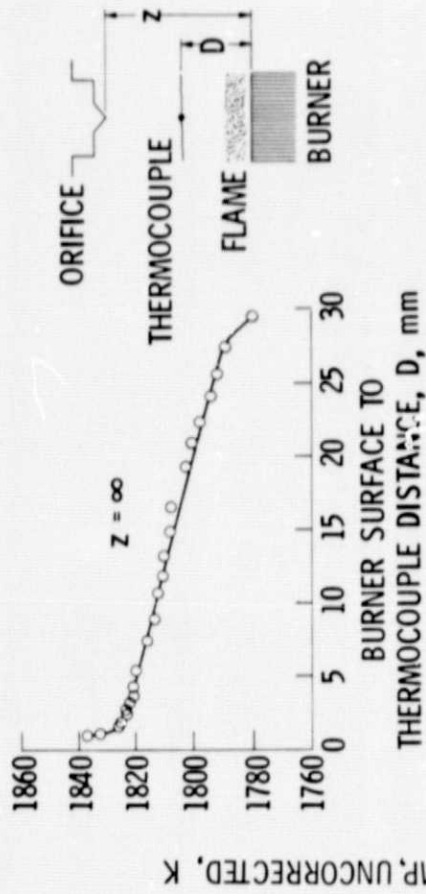


Figure 11. - Equilibrium chemical composition for  $K_2CO_3$ - $SO_2$ -doped  $CH_4$ - $O_2$  flame; potassium-containing species. Arrow indicates fuel/oxidant mass ratio of flame used.

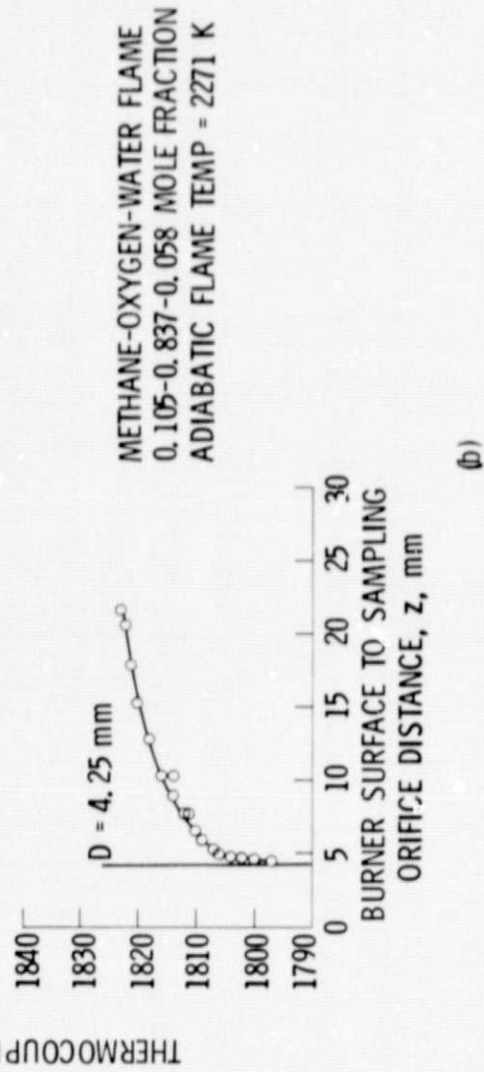


Figure 12. - Temperature profiles of  $CH_4$ - $O_2$  flame.